CORRELATION OF AEROELASTIC RESPONSE AND STRUCTURAL LOADS FOR HART II ROTOR USING LOOSE CFD/CSD COUPLING

Young-Hyun You, Jee-Woong Kim, Jung Hwan Sa, Jae-Sang Park, Soo-Hyung Park and Sung Nam Jung*

Dept. of Aerospace Information Engineering, Konkuk University
Hwayang-dong, Gwangjin-gu, Seoul 143-701, Republic of KOREA

Abstract

In this work, the comprehensive structural dynamics (CSD) code CAMRAD II is coupled with a computational fluid dynamics (CFD) code KFLOW to compute the rotor airloads, aeroelastic response, and structural loads of the HART II rotor in descending flight condition. A loose coupling methodology is adopted to combine the CFD and CSD codes. The convergence behavior of the CFD/CSD coupled analysis is investigated first by tracing the iteration histories of aerodynamic forces and moments, delta airloads, trim control angles, and blade structural motions, respectively. Next, a parametric study is demonstrated to assess the accuracy of the coupling analysis. This includes the refinement of CFD grid system and the influence of viscous boundary effects near the blade surface. The predicted results using the comprehensive analysis and Euler or Navier-Stokes CFD/CSD coupled analyses are correlated with the measured data. In general, the Navier-Stokes coupling results show better correlation than those by other methods. The contributing factors affecting the improvement of predictions are identified.

1. INTRODUCDTION

Even with the advanced computational power and state-of-the-art solution technologies, a reliable aeroelastic prediction of helicopter rotors is still a challenging task due to complex aerodynamic environment around the rotor disk and its strong interaction with the blade motions during the operation of helicopters. One crucial feature of the flow field is the blade vortex interactions (BVI), which generate the most annoying and intrusive noise from helicopter rotors [1]. The BVIs are caused by interactions between the rotor blades and their trailed vortices and these occur mainly in low speed transition, descent, and maneuvering flight conditions and cause significant noise and vibration problem. In order to understand the formation of vortex wakes and their interactions leading to noise and vibration, an international collaborative work, HART II [2], was conducted in 2001. Particularly, the goals of the test were to measure the noise level, airloads, vortex wakes, blade motions, and structural moments, with and without higher harmonic control (HHC) pitch inputs.

With the measured data set from the test, a variety of correlation studies have been carried out worldwide [3-11]. These range from low-order CSD (Comprehensive Structural Dynamics) methods [3-6], hybrid methods [7-8], and more involved CSD/CFD (Computational Fluid Dynamics) coupled approaches [9-11]. Most CSD codes adopt a lifting-line based aerodynamic model coupled with various levels of vortex wake representation, resulting in first-principle aeroelastic analysis solutions at a reasonable cost. This offers many advantages over other computationally heavier methods. However, it is generally conceived that the CSD approaches alone lack critical accuracy, especially in the prediction of vibration, loads, and noise level of helicopter rotors. Therefore, a high resolution CFD solver is required in any form and should be combined with CSD codes in the evaluation of the rotor flow fields.

Two different coupling algorithms are possible by combining the CFD and CSD codes in an interactive manner: loose coupling and tight coupling methods. The former has been pioneered by Tung et al. [12] through employing a so-called *delta airloads* technique. The loose coupling scheme assumes a periodicity of the solution and exchanges information between CFD and CSD codes on a per revolution base. This methodology has been successfully implemented by Potsdam et al. [13] for the validation of UH-60A rotor in different flight regimes. In the latter approach, the CFD and CSD codes are exchanged information at every physical time step for time accurate solutions. The tight coupling scheme is more general and desirable for aeroelastic stability, transient response, and non-periodic maneuvering flights. However, it is more time consuming and shows a difficulty in achieving trim conditions [14].

For modern CFD methodologies, much progress has been devoted toward reduction of numerical dissipation causing a diffusion of rotor vortices. Dietz et al. [15] used vortex-adapted Chimera-child grids to tackle the numerical dissipation problem of the trailing vortices and obtained improvements in tip vortex conservation. Brown et al. [16] applied the vorticity transport model (VTM) to separate the vorticity transport from the numerical dissipation of the Navier-Stokes solver. Recently, a three dimensional compressible Navier-Stokes slover KFLOW [17-19] has been exploited to validate the HART II data on structural responses [17] and vortex flow fields [18-19] and demonstrated reasonable accuracy solutions for the rotor.

The present work aims at extending the authors' previous HART II validation efforts and enhancing the prediction capability on airloads, aeroelastic response, and structural loads of the HART II rotor using a loose coupling strategy between CFD and CSD codes. For the coupling analysis, the CAMRAD II [20] is used to perform the structural dynamics calculation as well as the trim solution, while the KFLOW is adopted to compute the CFD airloads.

2. HART II TEST

The HART II test was conducted in the German-Dutch wind tunnel (DNW). The rotor was in descent flight conditions with an advance ratio μ = 0.15, a shaft tilt angle α_s = 4.5 deg. (after the wind tunnel wall correction), a hover tip Mach number M = 0.6387, and a thrust level C_T = 0.00457.

For the HART II rotor, 40% Mach-scaled models of the production BO-105 hingeless rotors were fabricated. The blade was dynamically scaled to match the natural frequencies of the first three flapping modes, the first two lag modes, and the first torsion mode of full-scale versions. The chord length was increased by 10% to compensate for the Reynolds number error. The blades had rectangular planform shape with -8 deg. linear pretwist and 2.5 deg. precone. The blades had a NACA23012 airfoil with a trailing-edge tab. The general properties of HART II blades are given in Table 1.

The cross-section of blades was composed of C-type spar, skin, and foam core. Both the skin and spar were made of glass fiber. The No. 1 blade in the rotor system was designated as the reference blade and defined the rotor azimuth. Each blade was instrumented with six strain gauges: three for flap, two for lead-lag, and one for torsion, while the reference and opposite blades (numbered one and three) were equipped with a root pitch sensor. The pitch link loads were also measured with a strain gauge attached to the pitch links. The deflections of HART II blades were measured optically using the SPR (Stereo Pattern Recognition) technique. To this purpose, 18 markers were distributed along the blade span and attached at both leading and trailing edges with an equal spacing starting from 22.8% radial location until the blade tip. The blade motions were defined with respect to the rotor hub. Both the flap and lead-lag motions were obtained based at the quarter chord line from the leading-edge of the blade [21].

3. NUMERICAL METHODS

3.1 CSD code: CAMRAD II

The CAMRAD II is a comprehensive aeromechanical analysis tool that is characterized by multibody dynamics, nonlinear finite elements, and various level of rotorcraft aerodynamic models [20]. For the structural analysis, the blade motion consists of the sum of the rigid body motion and the elastic deformation. The rigid body motion describes the motion of one end of a beam element, and the elastic motion is measured relative to the rigid motion. The beam elements are represented by three translational (axial, flap, and lead-lag) and three rotational degrees of freedom (DOF) that results in a fifteen DOF beam element.

The aerodynamic model used in CAMRAD II is based on a lifting-line theory combined with airfoil table look-up and the vortex wake. In addition, attached-flow unsteady aerodynamics along with various dynamic stall models is implemented in CAMRAD II. For the vortex wake model, the free wake geometry is used to compute the non-uniform induced inflow distribution around the rotor disk. The formation of the tip vortices is modeled using a simple rolled-up wake model or a multiple trailer with consolidation model. The rolled-up wake model is based on the feature that a tip vortex forms at the blade tip. Both single and dual peak models are available. It is remarked that the tip loss effect is neglected for the CFD/CSD coupled analysis.

3.2 CFD code: KFLOW

A three-dimensional compressible flow solver, called KFLOW [18], is used to obtain the computational fluid dynamics (CFD) airloads around the HART II rotor. The KFLOW is a parallelized multi-block structured, Navier-Stokes solver and is capable of computing time-accurate moving body problems by employing a Chimera overlapping grid system. A 2nd-order accurate, dual-time stepping technique combined with a diagonalized alternating-direction implicit (DADI) method is used to advance the solution in the time domain. The inviscid flux is calculated using the 5th order weighted essentially non-oscillatory (WENO) scheme and the central differencing technique is used to obtain the gradients of the viscous flux. The k-ω Wilkox-Durbin (WD+) scheme along with Spalart-Allmaras model is used for the turbulence model. Characteristic boundary conditions using the Riemann invariant are applied at the far field boundary, whereas a no-slip condition is applied at the solid wall of the blade.

In the aeroelastic simulation of a rotor system, the blade elastic deformations lead to changes in grid cell volumes, necessitating rigorous enforcement of the GCL (geometric conservation law), which states that the increase of a moving cell must be equal to the sum of the variations along the surface that encloses the volume [22]. The GCL is applied to meet the conservation relation on the surfaces and volumes of the control cells in a moving grid system. The elastic blade motions at each physical time step is updated using a modified volume calculated from the GCL.

3.3 CFD/CSD Coupling

Both CAMRAD II and KFLOW codes are used to construct a loose coupling framework for fluid-structure interactions. The key ingredient of the coupling is to exchange information between CFD and CSD codes on a per revolution base. To this end, the blade elastic motion data obtained from the comprehensive analysis are transferred to the CFD solver while the airloads data computed by CFD are passed back to the comprehensive analysis. Figure 1 shows the loose coupling strategy adopted in this study.

The coupling iteration begins with the comprehensive analysis using the lifting-line (LL) aerodynamics. At this stage, a single peak, rolled-up free wake model of CAMRAD II is used to describe the tip vortex characteristic of the rotor. The comprehensive analysis results containing the trim control angles and blade motion data are fed back into the CFD code to obtain the aerodynamic forces and moments (F/M) such as normal force (C_n), chordwise force (C_x), and pitching moment (C_m) of the rotor. The initial CFD run requires about three rotor revolution for a sufficiently converged solution. Next, the difference in airloads (i.e. delta airloads) obtained from CFD and CSD codes is calculated and processed until the airloads along with trim settings do not vary significantly from the previous coupling iteration. When the iteration terminates successfully (i.e. convergence is achieved), the low fidelity CSD airloads are fully replaced with the high precision CFD airloads.

It is remarkable that one and quarter (1.25) of a rotor revolution is seen to be enough for a converged CFD solution at any coupling iteration step when the previously obtained CFD solution is used as a restart condition. Hence, this reduced rotor run is applied throughout the coupling iterations except the first one to enhance the computational efficiency and also to maintain the numerical stability. In the comprehensive analysis, a simple uniform inflow model is used instead of the rather expensive free wake model, except the initial step where a single peak rolled-up wake model is used.

4. RESULTS AND DISCUSSION

The HART II measurement data are avialable for three different cases: baseline (BL), minimum noise (MN), and minimum vibration (MV). Only the BL case is considered for the present study.

4.1 CFD Grid system

A moving overlapped Chimera grid system with two different types of grids (blade grid and background grid) is employed to describe the flow field around the HART II rotor. Figure 2 shows a close-up view of the C-mesh topology grid around the blade and a perspective view of the grid system for the whole computational domain for the HART II rotor. The blade grids extend 1.5 times of the chord length away from the blade surface in all directions. The body grids are clustered near the leading edge, trailing edge, and blade tip regions. They are also clustered in the normal direction near the wall of the boundary. The background grids consist of an inner region that extends 4 chord lengths above, 3 chord lengths below from the rotor disk plane, and 1.5 chord lengths away from the blade tip. The inner region has a uniform spacing in all directions. The far field boundary extends 5 times larger than the blade radius from the rotor hub.

Three different grid systems are used in the current investiagtion: two of them are for Euler calculation and the last one is that for Navier-Stokes (N-S). Table 2 shows the details of the grid system used in the three cases. For example, the Euler I case uses a background grid spacing of 0.15c (15% of chord length) and consists of about 8.4 million cells. More specifically, the number of cells has a dimension of 169 x 97 x 21 (chordwise, spanwise, and normal) in the blade grid system, while the background grid has a dimension of 89 x 281 x 281 (downstream, lateral, longitudinal). The Euler II grids use the same blade grid set as the Euler I but with smaller back ground grid spacing (0.1c). In the Navier-Stokes grid, the number of blade grids is increased to capture the boundary layer effect near the blade surface while keeping the background grid system identical to the Euler I (0.15c).

Figure 3 shows the surface grids distributed over the isolated blades. It is noted that, in addition to the outboard main blade region that starts from 22% radial location to the tip, the inboard part of the blade is also modeled according to the description given by van der Wall [23]. The inboard region has rectangular section shapes having outer width 44 mm and outer height 16 mm with rounded corners. Both the hub and fuselage regions of the HART II configuration are neglected in the present analysis.

4.2 Convergence of CFD/CSD coupled analysis

The CFD/CSD coupled trim analysis is performed to match the measured trim targets specified in the HART II document. The overall trim process is handled by the comprehensive code. The target values to be met in the analysis are 3300 N, 20 N-m, and -20 N-m respectively for thrust, rolling, and pitching moments [21]. The rolling and pitching moments are defined as positive when the advancing side goes down and when the nose-up motion is induced, respectively. Figure 4a shows the change of trim values obtained for thrust, rolling and pitching moments with respect to the advancement of trim cycles. It is observed that a convergence is met after about six trim cycles are proceeded. The history of trim control angles is presented in Fig. 4b. It is indicated that the collective and cyclic control angles become converged within a few trim cycles, however, the trimmed cyclic values show some discrepancy with the measured trim settings. With the matched trim targets, the pitch control settings are obtained as: 3.18^o, 1.56^o, -0.72^o for collective (θ_0), lateral (θ_{1c}) and longitudinal (θ_{1s}) cyclic angles, respectively.

Figure 5 shows the CFD iteration history of the non-dimensionalized section normal force coefficient, M^2C_n, and pitching moment coefficient, M^2C_m, at 87% blade radial station, where M is the free stream Mach number. It is seen that the pitching moments become converged fast while the normal forces require about five to six iterations before they do not change significantly between the trim cycles. This fast converging trend of the pitching moment helps reaching a good convergence of the airloads solution. In order to judge a convergence of the CFD/CSD coupled analysis, the behavior of delta airloads are traced against the iteration trim cycles. Figure 6 shows the time history of delta airloads on the normal force, chord force, and pitching moment, respectively. It is noted that, in order to accelerate the computational efficiency of the CFD/CSD coupling, a rolled-up free wake model is adopted in the comprehensive analysis at the initial step of the coupling. But, in the subsequent stages of the coupling, a uniform inflow model is used throughout to speed up the coupling process. It is indicated in Fig. 6 that a good convergence is obtained after five to six coupling iteration cycles.

The coupled trim procedures should guarantee the convergence of the blade motions in any form. Figure 7 demonstrates the convergence characteristic of the coupled solution on the flap, lead-lag, and elastic twist deformations. As in the airloads cases, a good convergence is clearly obtained after five to six iteration cycles.

4.3 Parametric investigation

So far, the Euler I grid system has been used to check the convergence of the CFD/CSD coupled solution. In Figure 8, the predicted section normal forces (M^2C_n) and pitching moments (M^2C_m) denoted as dotted red lines are compared against the measured data denoted as a series of black dots. As can be seen, a 3 /rev behavior of the normal forces and the BVI peaks especially in the retreating sides are reasonably captured using the Euler I grid system with background grid spacing of 0.15c. However, the peak-to-peak magnitudes of the predicted normal forces are significantly over estimated and a phase shift is noticed in the second quadrant (from 90 to 180 deg.). In addition, the predicted pitching moments are underestimated significantly in the advancing side of the disk.

In a means to enhance the accuracy of the airloads predictions of the Euler solution, the background grid spacing is reduced to 0.1c (i.e. Euler II grid set). The results are presented together with the Euler I predictions in Fig. 8. It is observed that no significant improvement is obtained with the refined grid set except at or near the BVI events. This is not surprising considering the fact that the CFD background grid resolution affects mainly on the prediction and capturement of vortex wake. In order to investigate further the effect of grid resolution on the blade aeroelastic response, the flap, lead-lag, and elastic torsion deformations at the blade tip are presented as function of azimuth angles in Figure 9. Once again, the refined grids show a negligible influence on the blade response.

Based on the obsevation, the background grid spacing is set to 0.15c while the viscous effects are turned on in the following KFLOW computations. To this end, the blade grid system is modified and refined in the normal direction to capture boundary layer viscous effect in the vicinity of the blade surface (see Table 2). The first cell from the wall has a spacing of 10^{-5}. For computational efficiency, in the coupling between Navier-Stokes CFD and CAMRAD II, the Roe flux differencing splliting scheme is exceptionally used for the spatial discretization. After the convergence is met, however, two more iteration cycles are continued using the usual, fifth-order WENO scheme.

Figure 10 shows the comparison of the predicted Euler and Navier-Stokes computations on the section normal forces and pitching moments against the measured data of the HART II rotor. The Euler results are denoted as blue continuous line while the Navier-Stokes results are denoted as dotted red line. As can be seen, the correlation against the mesured data becomes greatly improved with the Navier-Stokes computations. Specifically, the larger peak-to-peak values in the Euler predictions are significantly reduced have a better correlation. A substantial increase of pitching moment in the advancing side of the Navier-Stokes predictions leads to a reduction of peak-to-peak values in the normal force. In addition, the phase shift problem encountered in the Euler predictions for the normal force is improved slightly. Actually, the shifting of phase is induced due to the change of trim control settings, as is indicated in Figure 11. In Figure 11, the trimed, rigid pitch angles obtained respectively from both Euler and Navier-Stokes calculations are presented together with measured values. The rigid ptich angle is defined as:

$$\theta = \theta_0 + \theta_{1c} \cos\psi + \theta_{1s} \sin\psi \qquad (1)$$

where ψ is the azimuth angle. Despite noticable improvement of phase shift in the Navier-Stokes predictions, there still remains phase discrepancy near 150 deg. of azimuth angles. It needs further investigation, but the measured target trim conditions might affect on the error. It is remarkable that Lim [11] used slightly different target trim values as compred with those used in the present study.

Figure 12 shows the comparison of airloads obtained from different CFD computations over the rotor disk. It is clearly indicated that one of the three peaks located near 120 deg. azimuth angles in the Euler predictions become redued significantly in the Navier-Stokes case.

4.4 Blade response and structural loads

Figure 13 shows the comparison of time variation of flap, lead-lag, and twist deformation at the blade tip between the CAMRAD II with rolled-up wake model and CFD/CSD coupling by Euler and Navier-Stokes methods, against the measured data. In the HART II test, the blade deflections are measured at 24 azimuth positions in increments of 15^{o}. Only the measured deflections of the reference blade (No. 1 blade) are compared, even though the test data show significant blade-to-blade dissimilarities [21]. It is defined as positive when the blade undergoes flap-up, lag-back, and nose-up deformation, respectively. The flap deflections are obtained by removing the precone angles from the vertical displacements, while the elastic twist deformation is obtained by subtracting the pitch control inputs and pretwist angles.

As is seen in Fig. 13, the correlation is generally good for flap deflections, but less satisfactory for elastic twist deformation. The peak-to-peak magnitudes of the flap deflections are matched best by the comprehensive analysis. For the twist deformation, the Navier-Stokes method improves the correlation significantly against the measured data, in both the peak-to-peak magnitude and the phase, in comparison with other analysis methods. For the lead-lag deflection, there is a constant offset amounting about 1/3 chord length between the measured and predicted results. Virtually, no diffence is observed among the predicted lead-lag deflections.

In the HART II, a total of six strain gauges were used to measure the blade structural loads. In this study, each of 15%, 14%, and 33% radial stations of the blade is chosen for the comparison of flap bending, lag bending, and torsion moments, respectively. It is defined as positive when the blades are bent up (flap bending), bent toward the leading-edge (lead-lag bending), and induced a pitch-up motion (torsion moment). It should be noted that the mean values of the structural moments were removed from the original test data, and only 1/rev and higher components are compared [11].

Figure 13 shows the comparison of the flap bending, lead-lag bending, and torsion moments at specified radial locations obtained by the different methods. In general, a significant improvement of correlation against the measured data is reached by the CFD/CSD coupled analysis. The peak-to-peak values of predicted flap bending moments by CFD/CSD coupled analysis become increased significantly to yield better correlation, as compared with the comprehensive predictions. The Navier-Stokes predictions demonstrate a clear improvement of torsion moments in terms of magnitudes and phases, as compared with those by the Euler and comprehensive methods.

5. CONCLUSION

In this work, a loose coupling approach between CAMRAD II (CSD) and KFLOW (CFD) codes was applied to predict the airloads, aeroelastic response, and structural loads of the HART II rotor. Three different grid sytems using either Euler or Navier-Stokes methods were employed to evaluate the accuracy of the CFD/CSD coupled analysis. The following conclusions were drawn from the present study.

1) In the loose coupling algorithm, about six trim iteration cycles were sufficient to reach convergent solutions on section forces and moments, delta airloads, and blade elastic motions of the HART II rotor.

2) The smaller background grid sizes would improve capturing more BVI peaks but no pronounced effects were obtained on the estimation of blade structural responses.

3) The Navier-Stokes methods demonstrated significant improvements of correlation on airloads, blade elastic twist response, and structural moments against the measured data, in terms of both magnitudes and phases. It was found that the closer agreement of section pitching moments played important roles for the better correlation in the Navier-Stokes predictions.

ACKNOWLEDGEMENT

This work was supported by National Research Foundation (NRF) through a grant provided by the Korean Ministry of Education, Science & Technology (MEST) in 2010 (No. K20601000001). The authors appreciate Dr. Do H. Kim at KARI for help in using CAMRAD II. The authors thank the HART II test

team for the data.

REFERENCES

[1] Yu, Y. H., Gmelin, B., Heller, H., Philippe, J. J., Mercker, E., and Preisser, J. S., "HHC Aeroacoustics Rotor Test at the DNW - The Joint German/French/US HART Project," *20th European Rotorcraft Forum*, Amsterdam, Netherlands, 1994.

[2] Yu, Y. H., Tung, C., van der Wall, B. G., Pausder, H. J., Burley, C., Brooks, T., Beaumier, P., Delriuex, Y., Mercker, E. and Pengel, K., "The HART-II Test: Rotor Wakes and Aeroacoustics with Higher-Harmonic Pitch Control (HHC) Inputs - The Joint German/French/Dutch/US Project," *58th Annual AHS Forum*, Montreal, Canada. June 11-13, 2002.

[3] J.-W. Lim, et al., "HART II: Prediction of Blade-Vortex Interaction Loading," *29th European Rotorcraft Forum*, Friedrichshafen, Germany, Sept. 16-18, 2003.

[4] H. Yeo, and W. Johnson, "Assessment of Comprehensive Analysis Calculation of Airloads on Helicopter Rotors," *Journal of Aircraft*, Vol. 42, No. 5, 2005, pp. 1218-1228.

[5] B. G. van der Wall, and J. Yin, "DLR's S4 Rotor Code Validation with HART II Data: The Baseline Case," *Int. Forum on Multidisciplinary Technology*, Seoul, Korea, Oct. 15-17, 2007.

[6] S. N. Jung, J.-S. Park, Y.-H. You, Y. H. Yu, J.-W. Kim, S. H. Park, and D.-H. Kim, "Comparison of Rotor Structural and Aerodynamic Loads Using the HART II Test Data," *35th European Rotorcraft Forum*, Hamburg, Germany, Sept. 22-25, 2009.

[7] M. E. Kelly, K. Duraisamy, and R. E. Brown, "Predicting Blade Vortex Interaction, Airloads and Acoustics using the Vorticity Transport Model," *AHS Specialists' Conference on Aeromechanics*, San Francisco, CA, Jan. 23-25, 2008.

[8] B.-Y. Min, L. N. Sankar, J. V. R. Prasad, and D. Schrage, "A Physics-based Investigation of Gurney Flaps for Rotor Vibration Reduction," *65th Annual AHS Forum*, Grapevine, Texas, May 27-29, 2009.

[9] M. Potsdam, H. Yeo, and W. Johnson, "Rotor Airloads Prediction using Loose Aerodynamic/ Structural Coupling," *Journal of Aircraft*, Vol. 43, No. 3, 2006, pp. 732-742.

[10] C. Yang, Y. Inada, and T. Aoyama, "BVI Noise Prediction using HART II Motion Data," *Int. Forum on Multidisciplinary Technology*, Seoul, Korea, Oct. 15-17, 2007.

[11] J.-W. Lim, "An Assessment of Rotor Dynamics Correlation for Descending Flight using CSD/CFD Coupled Analysis," *64th Annual AHS Forum*, Montreal, Canada, Apr. 29-May 1, 2008.

[12] C. Tung, F. X. Caradonna, and W. R. Johnson, "The Prediction of Transonic Flows on an Advancing Rotor," *Journal of the American Helicopter Society*, Vol. 31, No. 3, 1986, pp. 4-9.

[13] M. Potsdam, H. Yeo, and W. Johnson, "Rotor Airloads Predition Using Loose Aerodynamic/ Structural Coupling," *Journal of Aircraft*, Vol. 43, No. 3, 2006, pp. 732-742.

[14] P. Beaumier, M. Costes, B. Rodriguez, M. Poinot, and B. Cantaloube, "Weak and Strong Coupling Between the elsA CFD Solver and the HOST Helicopter Comprehensive Analysis," *31st European Rotorcraft Forum*, Florence, Italy, Sept. 13-15, 2005.

[15] M. Dietz, E. Kramer, and S. Wagner, "Tip Vortex Conservation on a Main Rotor in Slow Descent Flight Using Vortex-Adapted Chimera Grids," AIAA paper No. 2006-3478, 2006.

[16] R. E. Brown, and A. Line, "Efficient High-Resolution Wake Modelling using the Vorticity Transport Model," *AIAA Journal*, Vol. 43, No. 7, 2005, pp.1434-1443.

[17] S. N. Jung, J. S. Park, S. H. Park, and Y. H. Yu, "Validation of HART II Structural Dynamics Predictions Based on Prescribed Airloads," *AHS Specialists' Meeting on Aeromechanics*, San Francisco, CA, Jan. 20-22, 2010

[18] J. W. Sa, J. W. Kim, S. H. Park, J. S. Park, S. N. Jung, and Y. H. Yu, "KFLOW Results of Airloads on HART II Rotor Blades with Prescribed Blade Deformation," *2nd Int. Forum on Rotorcraft Multidisciplinary Technology*, Seoul, Korea, Oct. 19-20, 2009.

[19] J. W. Kim, J. W. Sa, S. H. Park, J. S. Park, S. N. Jung, Y. H. Yu, and K. W. Cho "Parallel CFD Computation for Vortex Flow Field around HART II Rotor Blades with Prescribed Blade Deformation," *Parallel CFD 2010*, Kaohsiung, Taiwan, May 17-21, 2010.

[20] W. Johnson, "CAMRAD II: Comprehensive Analytical Model of Rotorcraft Aerodynamics and Dynamics," Johnson Aeronautics, Palo Alto, CA, 1992.

[21] B. G. van der Wall, 2nd HHC Aeroacoustic Rotor Test (HART II) - Part I: Test Documentation, Institute Report IB 111-2003/31, German Aerospace Center (DLR), Braunschweig, Germany, 2003.

[22] P. D. Thomas, and C. K. Lombard, "Geometric Conservation Law and Its Application to Flow Computations on Moving Grids," *AIAA Journal*, Vol. 17, 1979, pp. 1030-1037.

[23] B. G. van der Wall, "The Data Base of the HART II International Workshop," Proc. Of ICEAE 2009, Bangalore, India, 2009.

TAB 1. General properties of HART II rotor blades.

Properties	Values
Number of blades, N_b	4
Radius, R	2.0 m
Root cutout	0.44 m
Chord length, c	0.121 m
Solidity, σ	0.077
Blade mass	2.24 kg
Lock number	8.06
Nominal rotor speed, Ω	1041 RPM

TAB 2. Specification of CFD grid system.

Cases	NB	OB	Total
Euler I (0.15c)	1.4M (169x97x21)	7.0M (89x281x281)	8.4M
Euler II (0.1c)	1.4M (169x97x21)	17.8M (111x401x401)	19.2M
N-S (0.15c)	3.2M (169x97x49)	7.0M (89x281x281)	10.2M

*M: million cells

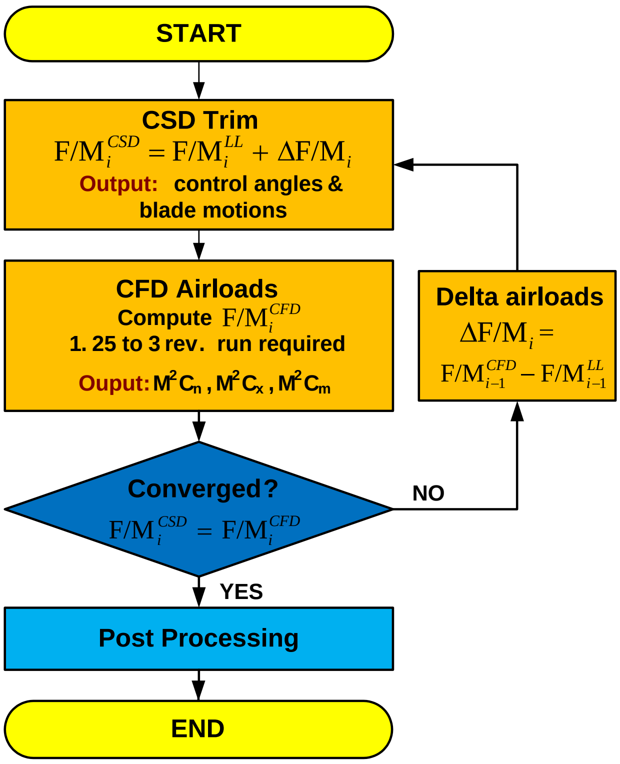

Fig. 1 Flow diagram of loose CFD/CSD coupling.

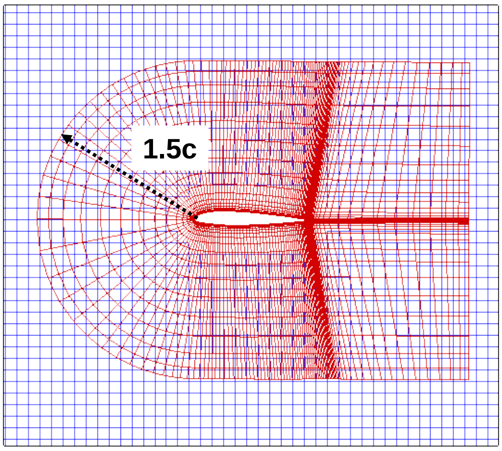

(a) Blade grid (Euler)

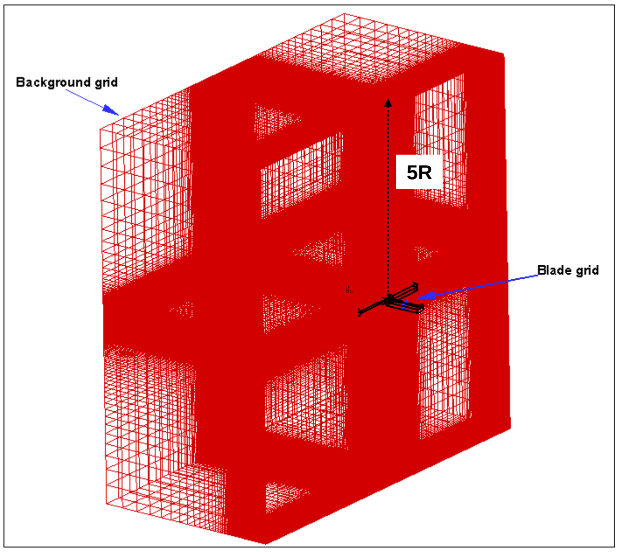

(b) Overall grid system

Fig. 2 Computational grid system of HART II rotor.

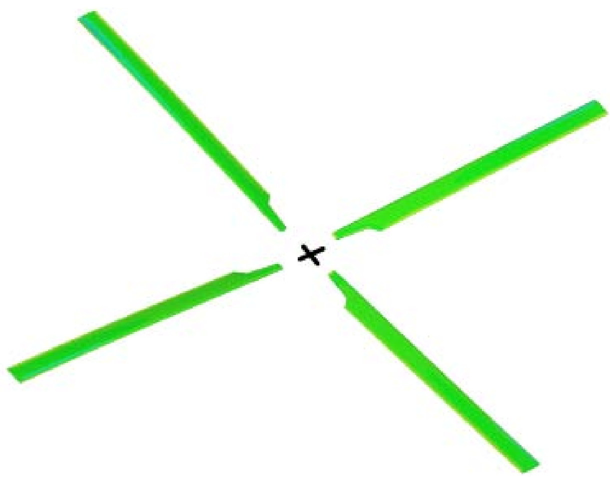

Fig. 3 Blade surface grids for HART II rotor.

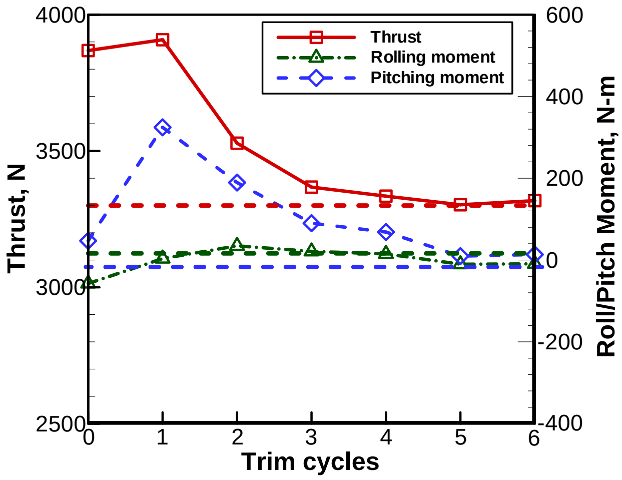

(a) Trim targets

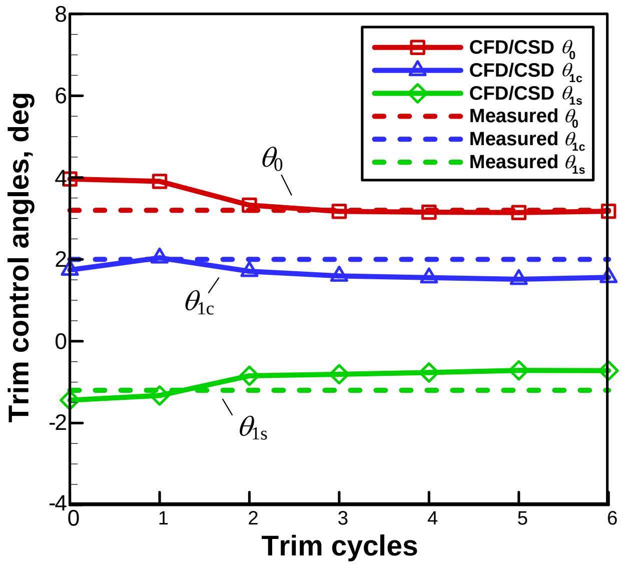

(b) Control trim angles

Fig. 4 Iteration history of trim targets and control angles of HART II rotor.

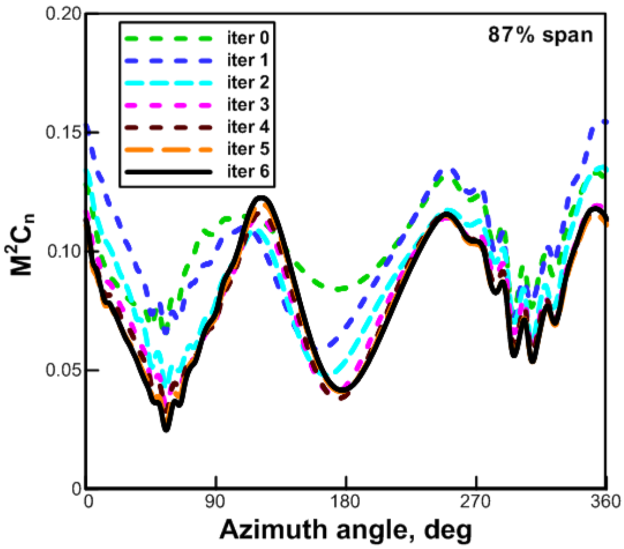

(a) Section normal force

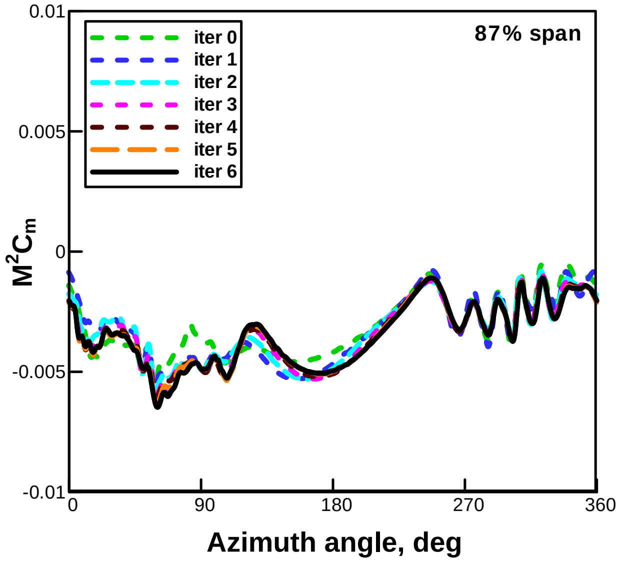

(b) Section pitching moment

Fig. 5 Iteration history of CFD/CSD coupled airloads.

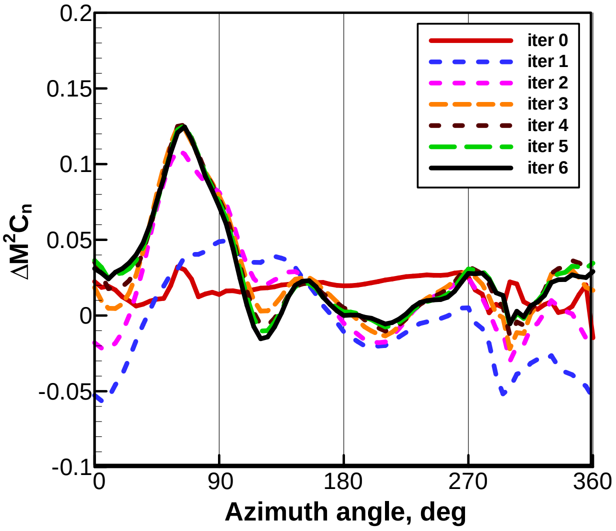

(a) ΔM^2C_n

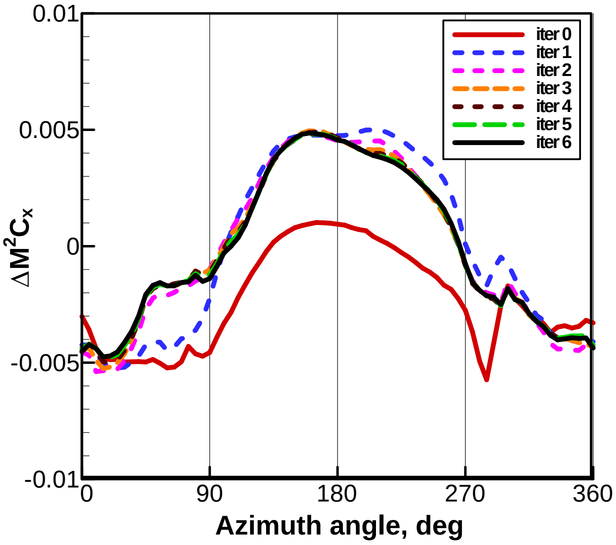

(b) ΔM^2C_x

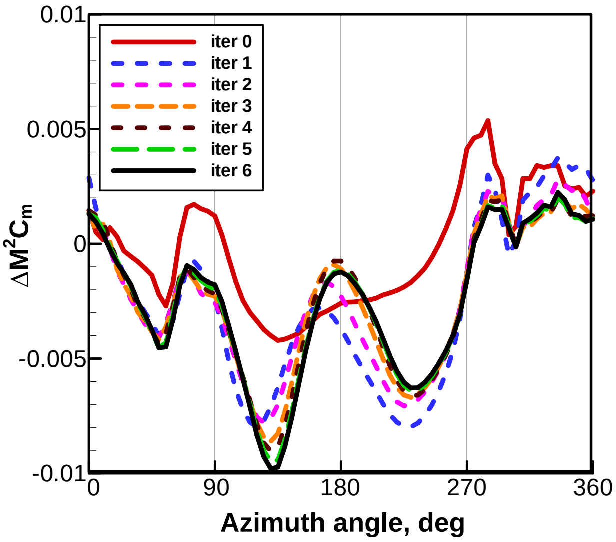

(c) ΔM^2C_m

Fig. 6 Iteration history of delta airloads.

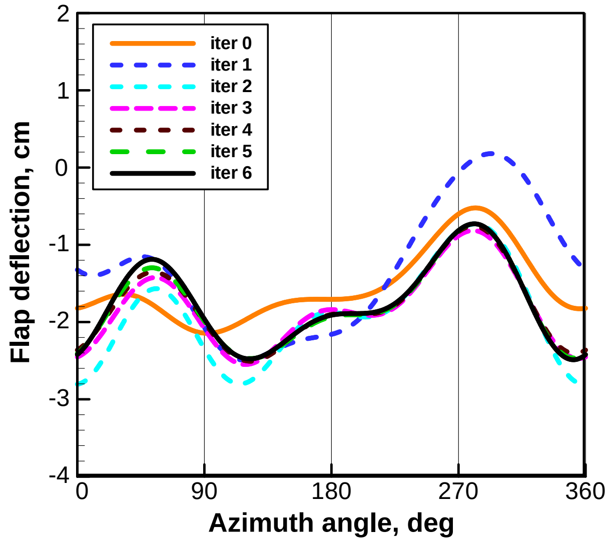

(a) Flap deflection

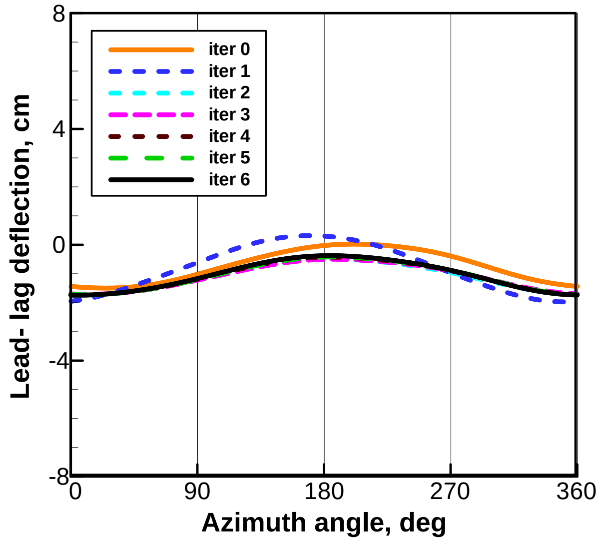

(b) Lead-lag deflection

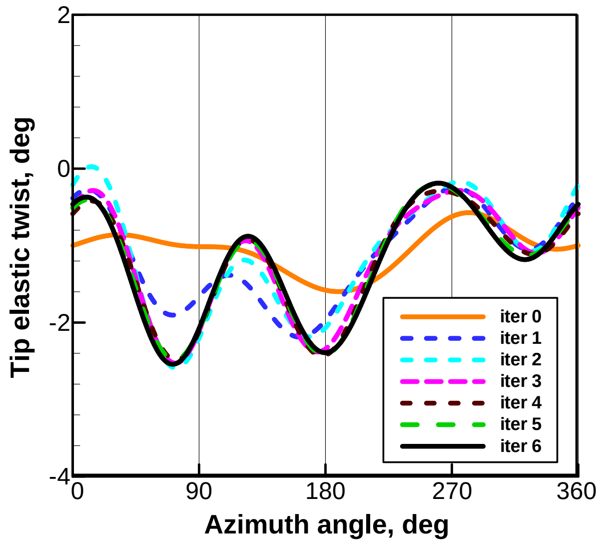

(c) Elastic twist deformation

Fig. 7 Iteration history of blade elastic motions.

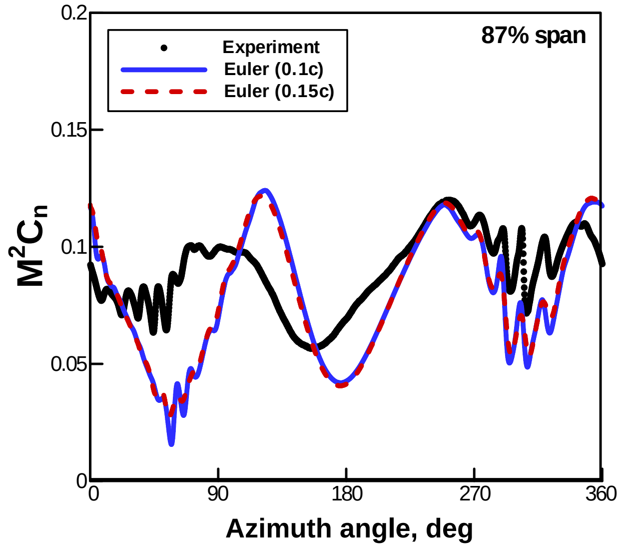

(a) M^2C_n

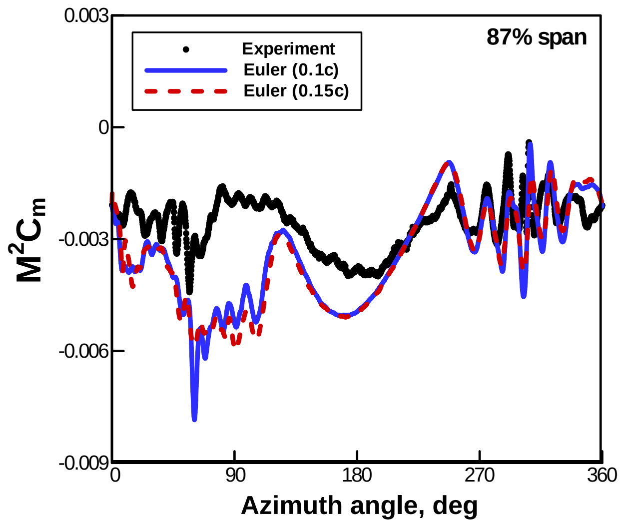

(b) M^2C_m

Fig. 8 Effect of grid resolution on section normal forces and pitching moments at 87% radial station.

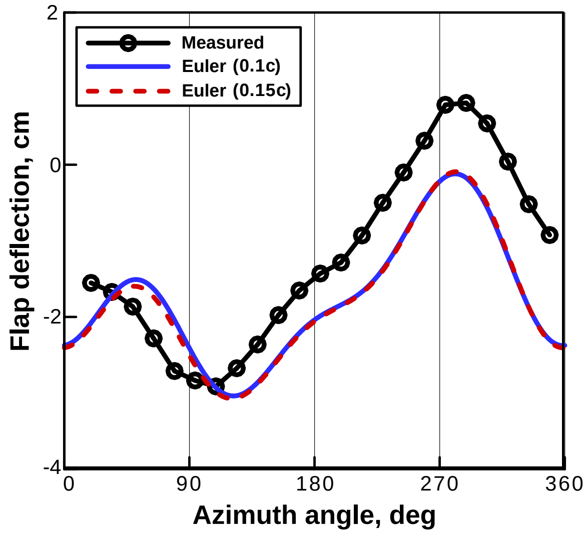

(a) Flap deflection

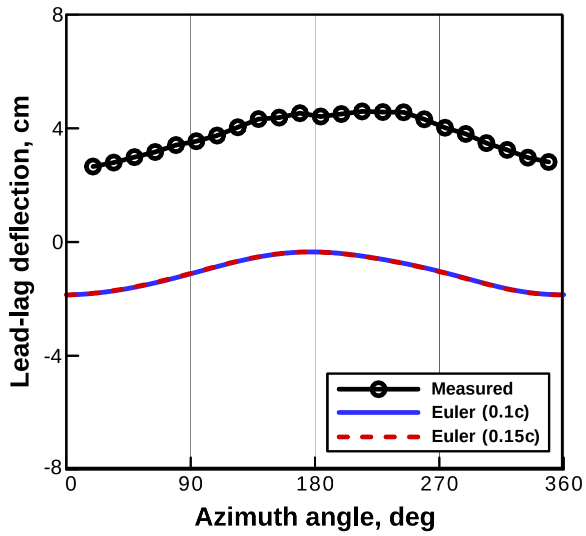

(b) Lead-lag deflection

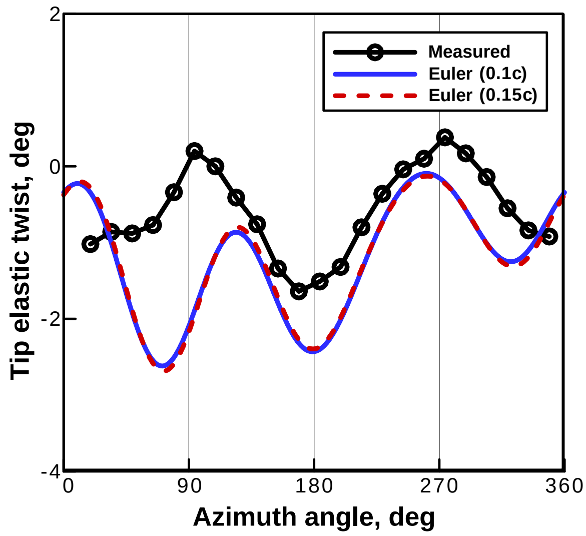

(c) Elastic twist angle

Fig. 9 Effect of grid resolution on blade deflections at 87% radial station.

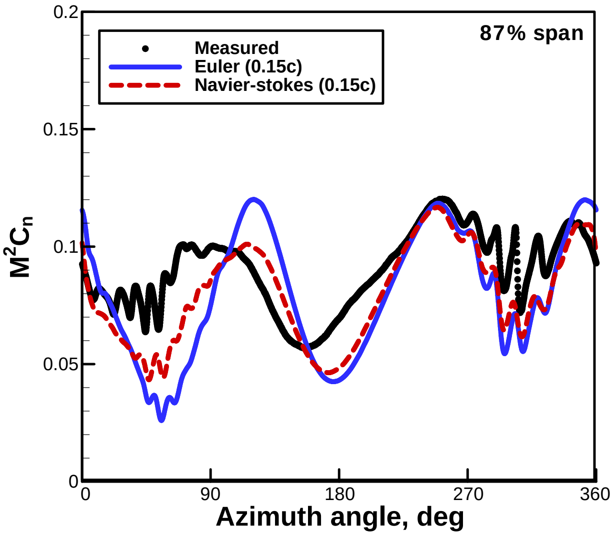

(a) Section normal force

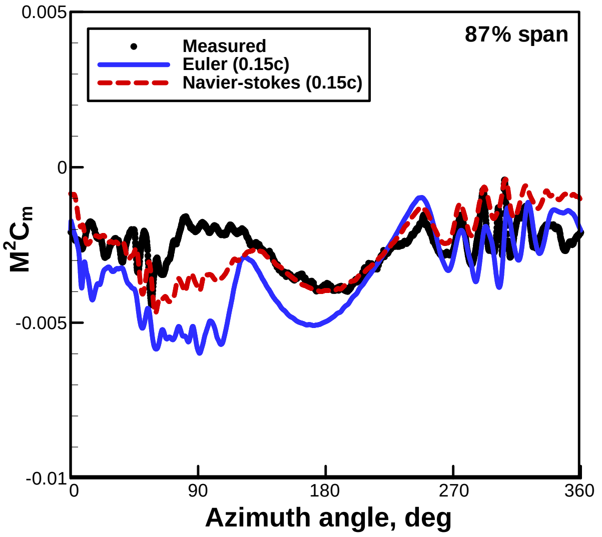

(b) section pitching moment

Fig. 10 Comparison of Euler and Navier-Stokes predictions for airloads at 87% radial station.

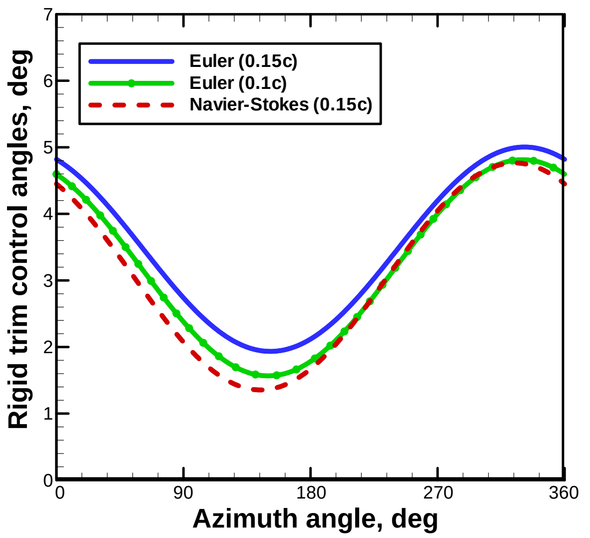

Fig. 11 Comparison of trim control angles.

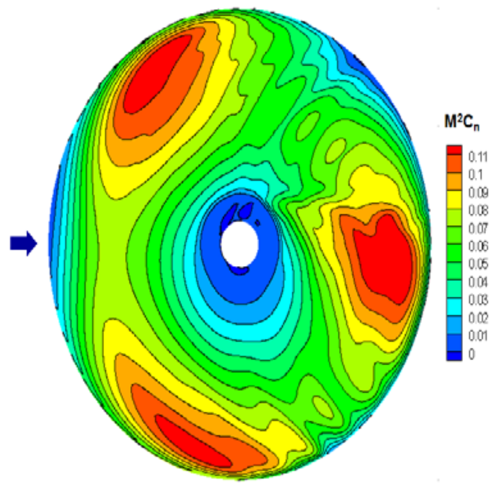

(a) Euler predictions (0.15c)

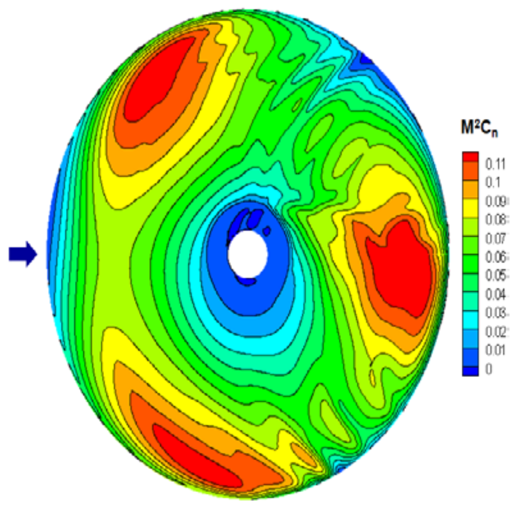

(b) Euler predictions (0.1c)

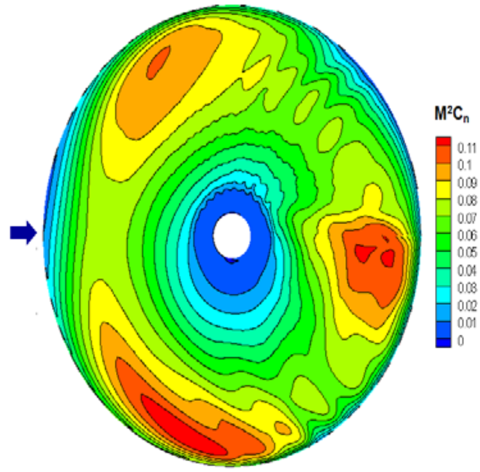

(c) Navier-Stokes predictions (0.15c)

Fig. 12 Comparison of airloads predictions over the rotor disk.

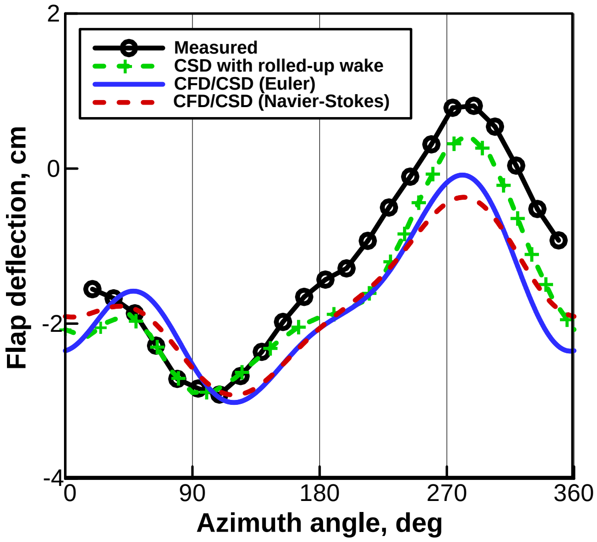

(a) Flap deflection

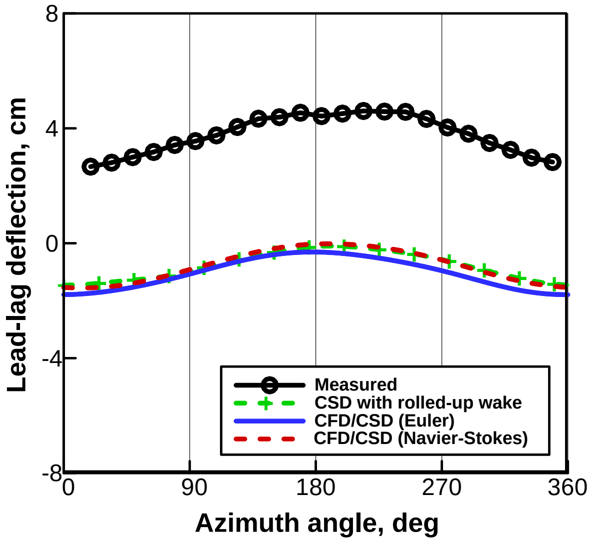

(b) Lead-lag deflection

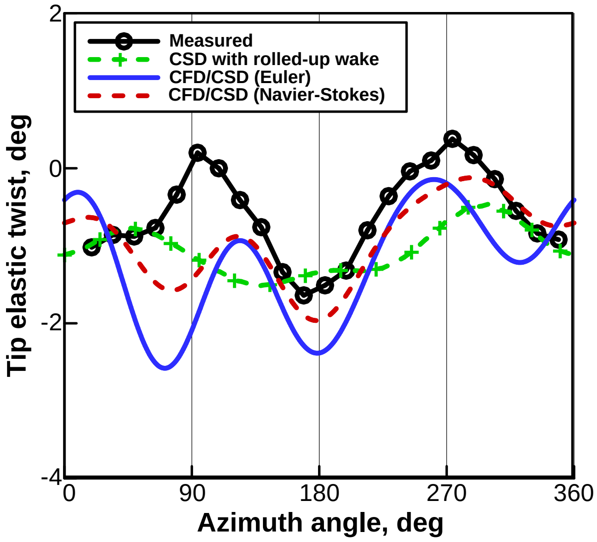

(c) Elastic twist angles

Fig. 13 Comparison of blade tip displacements.

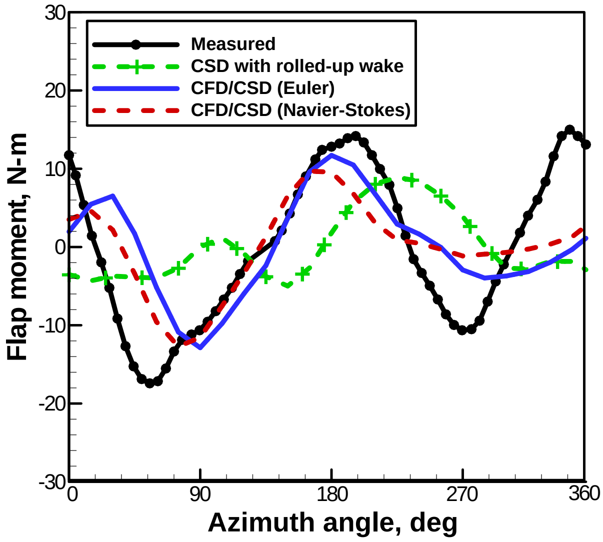

(a) Flap bending at 15% radial station

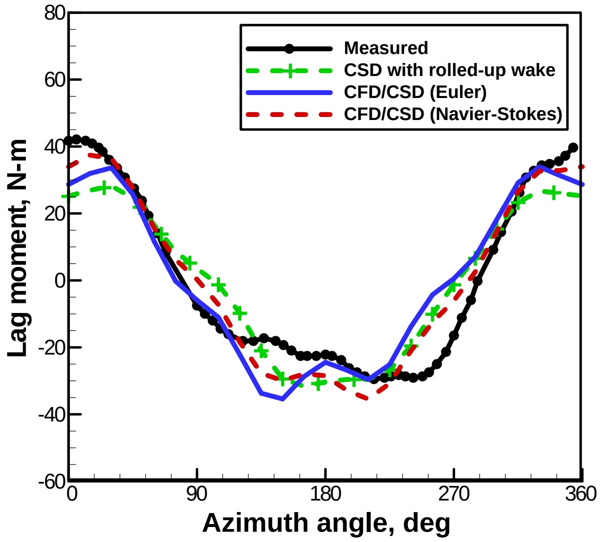

(b) Lead-lag bending at 14% radial station

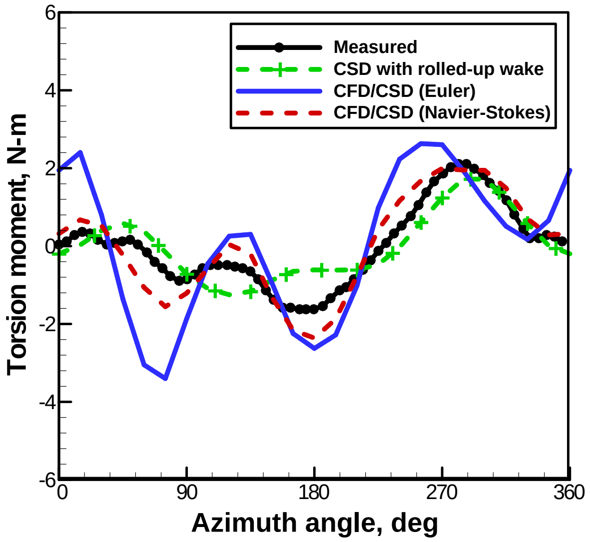

(c) Torsion moment at 33% radial station

Fig. 14 Comparison of blade structural moments.